AD-A095 282 MOORE SCHOOL OF ELECTRICAL ENGINEERING PHILADELPHIA PA F/G 7/4
EXPERIMENTAL AND THEORETICAL STUDIES OF DONOR-TYPE GRAPHITE INT--ETC(U)
DEC 80 J E FISCHER, S RABII DAAG29-77-C-0040

UNCLASSIFIED ARO-14625.14-P NL

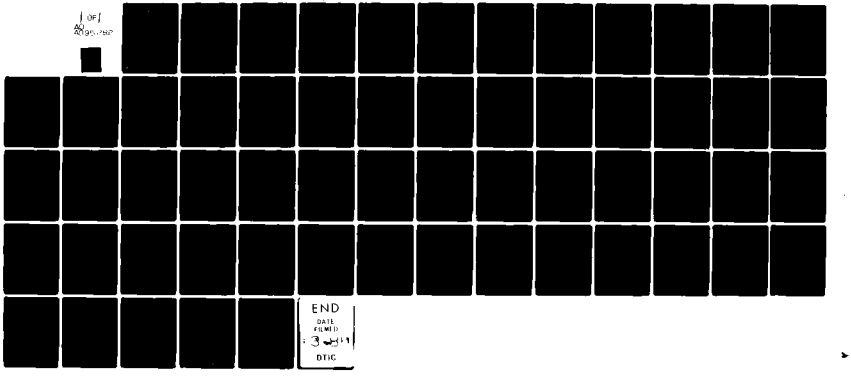

(12)

EXPERIMENTAL AND THEORETICAL STUDIES OF DONOR-TYPE GRAPHITE INTERCALATED COMPOUNDS

FINAL REPORT

J.E. FISCHER AND S. RABII

12/15/80

U. S. ARMY RESEARCH OFFICE

DAAG29-77C-0040

MOORE SCHOOL OF ELECTRICAL ENGINEERING
UNIVERSITY OF PENNSYLVANIA

THE VIEW, OPINIONS, AND/OR FINDINGS CONTAINED IN THIS REPORT ARE THOSE OF THE AUTHOR(S) AND SHOULD NOT BE CONSTRUED AS AN OFFICIAL DEPARTMENT OF THE ARMY POSITION, POLICY, OR DECISION, UNLESS SO DESIGNATED BY OTHER DOCUMENTATION.

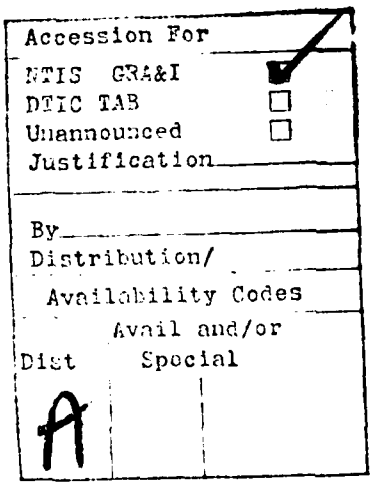

UNCLASSIFIED (18) ARO (19) 14625.14-P

SECURITY CLASSIFICATION OF THIS PAGE (When Data Entered)

REPORT DOCUMENTATION PAGE

READ INSTRUCTIONS BEFORE COMPLETING FORM

1. REPORT NUMBER

2. GOVT ACCESSION NO. AD-A095282

3. RECIPIENT'S CATALOG NUMBER

4. TITLE (and Subtitle) and Theoretical

(6) Experimental Studies of Donor-Type Graphite ~~Intercalation~~ Intercalated Compounds. (9)

5. TYPE OF REPORT & PERIOD COVERED rept. Jul 77-Sep 80 Final 7/77-9/80

6. PERFORMING ORG. REPORT NUMBER

7. AUTHOR(s)

(10) John E. Fischer and S. Rabii (15)

8. CONTRACT OR GRANT NUMBER(s) DAAG29-77C-0040

9. PERFORMING ORGANIZATION NAME AND ADDRESS
Moore School of Electrical Engineering
University of Pennsylvania
Philadelphia, PA

10. PROGRAM ELEMENT, PROJECT, TASK AREA & WORK UNIT NUMBERS

11. CONTROLLING OFFICE NAME AND ADDRESS
U. S. Army Research Office
Post Office Box 12211
Research Triangle Park, NC 27709

(11) 20

12. REPORT DATE December 1980

13. NUMBER OF PAGES

14. MONITORING AGENCY NAME & ADDRESS (if different from Controlling Office)

(12) 58

15. SECURITY CLASS. (of this report) Unclassified

15a. DECLASSIFICATION/DOWNGRADING SCHEDULE

16. DISTRIBUTION STATEMENT (of this Report)

Approved for public release; distribution unlimited.

17. DISTRIBUTION STATEMENT (of the abstract entered in Block 20, if different from Report)

NA

18. SUPPLEMENTARY NOTES

The view, opinions, and/or findings contained in this report are those of the author(s) and should not be construed as an official Department of the Army position, policy, or decision, unless so designated by other documentation.

19. KEY WORDS (Continue on reverse side if necessary and identify by block number)

graphite, intercalation, band structure, electronic properties

20. ABSTRACT (Continue on reverse side if necessary and identify by block number)

DD FORM 1 JAN 73 1473 EDITION OF 1 NOV 65 IS OBSOLETE

UNCLASSIFIED

SECURITY CLASSIFICATION OF THIS PAGE (When Data Entered)

237000

INTRODUCTION

This final report covers the period August 1, 1977 to September 30, 1980. It really isn't final, since work will continue under a new contract (DAAG29-80-K-0019) which carries the title "Fundamental Electronic Properties of Donor-Type Graphite Intercalated Compounds"

Since all the significant results have been published in the open literature, we present here the highlights of those results. Attached as appendices are preprints of papers which are not in print as of this writing.

STATEMENT OF PROBLEM

Graphite intercalation compounds are a large family of quasi-two dimensional synthetic metals. Fundamental interest centers on their unusual crystal structures and their effects on electronic properties. Practical applications are envisaged as lightweight conductors of electricity.

The goals of this program are to understand the electronic structure of donor-type compounds, with a view toward obtaining detailed correlations between chemical and physical variablles. Emphasis is placed on the one-electron spectrum, transport and optical properties and charge distributions. Synthetic methods are developed to provide high-quality specimens for a variety of physical measurements. Band theoretical techniques are applied to develop models for the electronic structure. Iteration between theory and and experiment leads to more sophisticated models.

HIGHLIGHTS

1. It had been known for some time that the Hall coefficient of KC_8 and related materials was anomalously small at room temperature, implying a free electron density in excess of the metal atom density if one chose to interpret R_H with a one-carrier model. We found from low temperature measurements that the hall coefficient changes sign, becoming p-type in the helium range. This suggested a two-carrier model for the transport process, in which electrons and holes are nearly compensated at room temperature. For the reflectance spectra, a two-carrier model was also required to obtain a good fit to the data, as well as to obtain agreement between optical parameters and the dc conductivity. This interpretation remains somewhat controversial, in the sense that the Japanese group under Prof. Tanuma do not find a positive Hall coefficient at low temperature. We simply point out that the resistance ratios of our samples are of order 200-300, while Tanuma's samples are of order 10.

2. With the publication of band structures for KC_8 and LiC_6, by the Japanese and ourselves respectively, it became apparent that the different in-plane symmetries of intercalant layers in these two materials might be playing an important role in determining the overall electronic properties. In KC_8, the metal s electrons were found to hybridize strongly with the carbon p_z electrons near the Fermi energy, giving rise to two types of carriers (in agreement with the data mentioned above). In LiC_6, on the other hand, no evidence was found for $s\text{-}p_z$ mixing near E_F. At the time, LiC_6 was a difficult material

experimentally, due to limitations in the available synthetic methods. We proceeded to develop simplified techniques for making LiC_6 and the stage two compound "LiC_{12}", and to supply samples of these materials to many groups for a wide variety of experiments.

3. We found that the temperature dependence of resistivity in the heavy alkali compounds could be fit to the sum of a linear and a quadratic term, the linear term representing usual electron-phon scattering while the quadratic term was interpreted as either electron-hole or electron-electron scattering in a complex Fermi surface. This interpretation agreed with the band structure work noted above, in that the T^2 term was much larger in stage one materials than in stage two.

4. In collaboration with DiSalvo and Safran at Bell Laboratories, we performed total susceptibility measurements on stages one, two, three and four potassium samples. Surprisingly, we found that the susceptibility for magnetic fields along the c-axis increased with stage, contrary to what would be expected if the origin of the susceptibility were simply Pauli paramagnetism. This effect was ultimately traced to an unusual Landau paramagnetism which turns out to be characteristic of "doped" two-dimensional graphite. In other words, if in a high stage compound the transferred electrons are mainly localized on carbon layers neighboring the metal layers, then these carbon layers will exhibit an anomalously large orbital paramagnetism. The interior layers, those far from a metal layer, are more nearly like pure graphite, and should ultimately (at some very high stage) exhibit the large orbital

diamagnetism associated with the degenerate semimetallic nature of pure graphite. It was realized that by extending these measurements to more dilute materials, one might be able to map out the $\bar{c}$-axis charge distribution in detail.

5. We performed a detailed band structure calculation for LiC_6, choosing this compound for its simple crystal structure. A Green's function technique with non-muffin-tin corrections was used, and approximate self-consistency was checked by comparing results from atomic and fully ionic potentials. This calculation is now widely accepted by workers in the field, because of the many aspects in which it agrees with experiment:

- The calculated density of states at the Fermi energy $N(E_F)$ agrees with the low temperature linear term in specific heat to better than one percent.

- The metallic reflectivity spectrum is fit very well by the theoretical plasma frequency and a reasonable core dielectric constant.

- The anisotropy in the conductivity at room temperature agrees well with the calculated anisotropy of the plasma frequency, implying that the scattering time is essentially isotropic.

- The experimental values for Knight shift and Pauli susceptibility are consistent with the theoretical value for the contact density of s electrons.

- The angle resolved photoemission spectrum of LiC_6 is in excellent agreement with the calculated energy band structure.

6. The theoretical techniques developed for LiC_6 are being applied to the first-stage potassium compound KC_8. The energy band picture is substantialy completed and the results indicate that the bottom of K 4s band lies $\sim$1.5 eV above the Fermi level. This indicates that the Fermi surface will lack the central isotropic pocket of carriers predicted by other studies. A series of saddle point transitions centered at 4.1 eV, appear consistent with the low energy electron loss spectra.

7. A similar theoretical study of pur graphite was initiated to test the technique used for LiC_6 and KC_8 on a better known material. The initial picture of the energy bands is in good agreement with those obtained by other techniques.

PERSONNEL

Prof. J. E. Fischer	P/I
Prof. S. Rabii	P/I
Dr. Margerita Zanini	
Dr. Wayne Johnson	
Dr. Natalie Holzwarth	Postdoctoral
Dr. Michael Moran	Fellows
Dr. Samar Basu	
Mark Potter	(MSEE 12/78)
David DiVincenzo	(PhD Student)
Robert Tatar	(PhD Student)
Carl Fuerst	(PhD Student)
Richard Grayeski	(Student Assistant)

PUBLICATIONS

1. "Alternate Synthesis and Reflectivity Spectrum of Stage 1 Lithium-Graphite Intercalation Compounds", M. Zanini, S. Basu and J. E. Fischer, Carbon 16, 211 (1978)

2. "Raman Scattering in LiC_6: Evidence for a Rigid Band Interpretation", M. Zanini, Lih-Ying Ching and J. E. Fischer, Phys. Rev. B18, 2020 (1978).

3. "Graphite Intercalation Compounds", J.E. Fischer and T.E. Thompson, Physics Today, 31, 36 (1978).

4. "Optical Anisotropy of HOPG: Effect of Surface Preparation", M. Zanini, D. Grubisic and J. E. Fischer, Phys. Stat. Sol. (b) 90, 151 (1978).

5. "Graphite Intercalation Compounds: An Overview", J. E. Fischer, Comments in Solid State Physics, 8, 155 (1978).

6. "Anisotropic Magnetic Susceptibility and Phase Transitions in Intercalated Graphite: KC_{24}", F.J. DiSalvo and J. E. Fischer, Solid State Comm. 28, 71 (1978).

7. "Anisotropy of Graphite Intercalation Compounds", J. E. Fischer, in "Molecular Metals", W. E. Hatfield, editor, Plenum Press, New York (1979) p. 281.

8. "Electronic Properties of Graphite Intercalation Compounds", chapter in Physics and Chemistry of Materials with Layered Structures, (F. Levy, editor) D. Reidel, Holland, Vol 6 p. 481 (1979).

9. "Intercalated Graphite: Some Aspects of Two-Dimensionality", J. E. Fischer, Comments on Solid State Physics, 9, 93 (1979).

10. "Preparation and Properties of Lithium-Graphite Intercalation Compounds", S. Basu, C. Zeller, P. Flanders, C.D. Fuerst, W. D. Johnson and J. E. Fischer, Mat. Sci. Eng. 38, 275 (1979).

11. "Large Anisotropy and Stage Dependence of the Magnetic Susceptibility of Alkali Graphite Compounds", F.J. DiSalvo, S.A. Safran, R. C. Haddon, J. V. Waszczak and J. E. Fischer, Phys. Rev. B20, 4883 (1979).

12. "Raman Scattering in Graphite Lithium Intercalation Compounds" P. C. Eklund, G. Dresselhaus, M. S. Dresselhaus and J. E. Fischer, Phys. Rev. B21, 4705 (1980).

PUBLICATIONS

13. "Interlayer Screening and Magnetic Susceptibility of Graphite Intercalation Compounds", S. A. Safran, F. J. DiSalvo, R. C. Haddon, J. V. Waszczak and J. E. Fischer, Physica B, 99, 494 (1980).

14. "Graphite Intercalation Compounds", J. E. Fischer, Physica B 99 , 383 (1980).

15. "Specific Heat of LiC_6 from 4-300K", C. Ayache, E. Bonjour, R Lagnier and J. E. Fischer, Physica B 99, 547 (1980).

16. "Elastic and Inelastic Neutron Scattering Studies of Lithium-Graphite", J. Rossat-Mignod, D. Fruchart, M.J. Moran, J. W. Milliken and J. E. Fischer, Synthetic Metals (to be published).

17. "The Electronic Structure of KC_8" D. P. DiVincenzo, N.A.W. Holzwarth and S. Rabii, Physica 99B, 406 (1980).

18. "Energy Band Structure of Three Dimensional Graphite", R. C. Tatar, N.A.W. Holzwarth, and S. Rabii, Journal of Synthetic Metals (accepted for publication).

19. "A Calculation of the Electronic Band Structure of KC_8" D. P. DiVincenzo, N. A. W. Holzwarth and S. Rabii, Journal of Synthetic Metal (accepted for Publication).

20. "Transport Properties of Alkali Metal-Graphite Intercalation Compounds" M. E. Potter, W. D. Johnson and J. E. Fischer, Solid State Communications (submitted).

NEUTRON SCATTERING STUDY OF LITHIUM-GRAPHITE INTERCALATION COMPOUNDS*

J. Rossat-Mignod, D. Fruchart
Centre d'Etudes Nucleaires
38041 Grenoble, France

and

M.J. Moran†, J.W. Milliken, J.E. Fischer
Moore School of Electrical Engineering and
Laboratory for Research on the Structure of Matter**
University of Pennsylvania
Philadelphia, PA 19104

ABSTRACT

Elastic and inelastic neutron scattering are reported for stage 1 and 2 Li-graphite. The principal results are as follows:

1. No evidence was found for the previously reported stacking transition in LiC_6; the normal $A\alpha A\alpha$ ... stacking persists down to 10K.
2. The C-parameter of LiC_6 increases rapidly with increasing T (1.5% between 300 and 490K). This may be a precursor to the Li order-disorder transition which occurs above 500K.
3. Upon heating above 520K, stage 2 transforms into a dilute stage 1 phase, as predicted by Safran.
4. The dispersion of the LA phonon propagating along $\bar{c}$ shows a 40% increase in sound velocity relative to pure graphite, as compared to 10% for RbC_8. This confirms the existence of strong interlayer interactions in LiC_6.

INTRODUCTION

Several papers at this conference deal with phase transitions in various compounds. Such studies are important both in terms of expanding our knowledge of intercalated graphite[1] and as they apply to general issues in critical phenomena. Bak[2] has demonstrated the isomorphisms between prototypical GIC's and idealized model lattices whose critical behavior have been predicted theoretically. Experiments on GIC's therefore, can serve as a basis for testing these theories.

We report here the preliminary results of a neutron scattering study of phase transitions and phonon spectra in stages 1 and 2 Li-graphite. Large ($\sim$1 gram) samples were prepared from HOPG by liquid phase synthesis[3] and sealed in quartz or stainless steel tubes along with He exchange gas. Since the isotope ^{6}Li (4% abundant) is a strong absorber for thermal neutrons, we used 99+% enriched ^{7}Li. Neutron scattering experiments were performed on a triple axis spectrometer at the Siloe reactor in Grenoble. Pyrolitic graphite was used as monochromator, analyzer and filter. A wavelength of 2.4 A was used for the elastic diffraction studies. The sample was placed in either a He cryrostat or an oven, with $\vec{c}$-axis in the scattering plane.

SEARCH FOR STACKING TRANSITION

At 300K the Li atoms in LiC_6 form a triangular lattice commensurate with the hexagonal array of carbon atoms. The unit cell is hexagonal with $a=a_o\sqrt{3}$, where a_o is the graphite in-plane parameter. All Li layers are equivalent, as are all C layers, so the alternate stacking in stage 1 can be written $A\alpha A\alpha\ldots$, A denoting carbon and α denoting Li layers.[4] Kambe et. al.[5] recently reported a transition to a more complex stacking upon cooling below 200K. They interpreted their electron diffractograms for T<200K in terms of $A\alpha A\beta A\gamma\ldots$. stacking, based on the disappearance of (h,0,0) diffraction spots, the only remaining spots being $(h\sqrt{3},0,0)$, i.e. those due to the graphite in-plane structure.

With a view toward studying this transition in more detail, we recorded (0,0,ℓ), (h,0,0) and (1,0,ℓ) diffraction scans at 10, 200 and 300K. To our surprise, no transition was observed. A sampling of the data is shown in Fig. 1. The top panel shows a (1,0,ℓ) scan at 10K. The Bragg peaks at ℓ=0, 1 are characteristic of the hexagonal cell, i.e. $A\alpha A\alpha\ldots$ stacking. If a transition to $A\alpha A\beta A\gamma$ had occurred, the unit cell would now be rhombohedral, leading to extintion of the ℓ=0, 1 peaks and the appearance of new peaks at ℓ=1/3, 2/3 (both occurring due to the powder averaging of in-plane scattering in HOPG). The middle and lower panels show (h,0,0) scans at 200K and 10K. Here, the fact that the (1,0,0) and (2,0,0) intensities do not change upon cooling also signifies the absence of a stacking transition.

For both scans the 300K data are identical to the 10K results, and two samples behaved identically. We conclude that the ground state structure is the same as the 300K one first reported by Guerard and Herold,[4] and that some other phenomenon must be invoked to explain the electron diffraction results.[5]

It must be pointed out, however, that despite the discrepancy between electron and neutron diffraction results, weak anomalies have been observed in specific heat[6] and basal plane conductivity[3] at temperatures corresponding to the change in electron diffraction pattern. On the other hand, no effect was found in differential scanning calorimetry.[5]

HIGH-TEMPERATURE RESULTS

Diffraction scans were recorded for a LiC_6 sample sealed in quartz, as a function of increasing temperature. Unfortunately the container failed before reaching the order-disorder transition, evidently due to a trace of free Li which attacked the quartz. However, the elastic scans revealed a very large thermal expansion in the $\bar{c}$-direction, shown in Fig. 2. The expansion is nonlinear, and the rate increases with increasing T. Over the same interval the $\bar{a}$-parameter is constant within experimental error ($\Delta a/a < 5 \times 10^{-6}/K$). This suggests anomalously large out-of-plane thermal motion of Li as the order-disorder transition is approached.

A second sample was packaged in a stainless steel tube thinned to 0.007 inches to minimize the background scattering. This sample also suffered from an unplanned event during heating, namely the failure of a thermocouple which led to a temperature excursion above 650K.

Upon cooling to room temperature, it was found that the sample had irreversibly transformed to a mixture of stage 2 (presumably LiC_{12}) and lithium carbide Li_2C_2. After repairs, the stage 2 phase was studied as a function of increasing T. Figure 3 shows the temperature variation of the integrated (0,0,1) peak of "LiC_{12}" (this corresponds to ℓ=0.52 in units of the LiC_6 cell). The transition is clearly a higher order phenomenon with large hysteresis. The remaining intensity at 150-200C is due to a new expanded stage 2 phase (LiC_{18}?). By 250C the only remaining (0,0,ℓ) intensity is indexable as stage 1, but with $\bar{c}$ parameter $\sim$1% smaller than that of LiC_6 at that temperature. Scans along (h,0,0) at 250C show that the Li layer is now disordered. We conclude that the net effect over the range 100C - 250C is the transformation of ordered, close-packed stage 2 to dilute stage 1 with liquid-like Li layers, as predicted by Safran.[7] A dilute stage 2 intermediate phase seems to occur as the stage 1 grows at the expense of "dense" stage 2. This effect is completely reversible. We plan to repeat this experiment on a well-characterized LiC_{12} sample.

PHONONS

Inelastic neutron scattering of LiC_6 was performed at 200K in a geometry which reveals only longitudinal modes propagating in the $\bar{c}$-direction. Figure 4 shows the loss spectra for two $\bar{q}$-values. Two loss peaks are observed, both of which increase in energy with increasing $\bar{q}$. The lower energy peak decreases in intensity with increasing $\bar{q}$, and is no longer observed beyond $\bar{q}=0.3(2\pi/\bar{c})$.

Figure 5 shows the dispersion of these two modes. The upper mode extrapolates to zero energy at $\bar{q}=0$, so we assign it to the LA phonon. On the other hand, the lower mode tends toward a value 1-2 meV (8-16K) at $\bar{q}=0$, so we tentatively assign this branch to an LO mode.

The LA mode can be compared directly to the corresponding branches in graphite[8] and RbC_8[9]. From the initial slopes we find that the $\bar{c}$-axis sound velocity of LiC_6 is enhanced 40% relative to graphite, whereas RbC_8 is enhanced only 10%. This in turn implies a relatively large interlayer interaction in LiC_6, which is consistent with many independent observations:

1) The observed layer spacing is only 83% of the hard-sphere estimate, suggesting strong covalency[10].
2) Theoretical charge density indeed reveals a pileup between C and Li layers[11].
3) The conductivity anisotropy σ_a/σ_c is only 10 at 300K[3].
4) The lattice specific heat[6] goes as T^3 (i.e. three-dimensional) up to 50K, whereas in graphite the T^3 region extends only to ~4K.

The putative LO mode is harder to explain. No similar mode was found in RbC_8, so we are led to suspect that the small mass of Li is implicated. One possibility would be a ferroelectric instability whereby at low T the Li atoms are located in two local potential minima straddling the mid-plane.

The barrier between these two wells would correspond to the $\bar{q}=0$ "gap" of the LO branch, i.e. $\sim$10K. Above 10K, thermal motion would produce a structure in which, on average, the Li layer is equidistant between flanking carbons, as observed. This hypothesis is subject to verification by looking for a displacive transition of Li layers below 10K, and by determining the temperature dependence of the LO mode.

A second possibility is that the mode results simply from the Li-carbon interaction, which, among other things, could mix some of the low-lying modes which occur in graphite. Calculations[8] show that the TO and LA modes in pure graphite cross each other halfway from $\bar{q}=0$ to the zone boundary. It is conceivable that in LiC_6 these graphitic branches produce a low-lying mode with a small gap at $\bar{q}=0$. This hypothesis can be tested by a lattice dynamics calculation for LiC_6

We acknowledge fruitful discussions with D. Guerard, J.Y. Henry and S. A. Solin.

REFERENCES

* Supported in part by ARO contract DAAG29-77-C-0040.

† Present address: Naval Research Laboratory, Washington, DC 20375

** Supported by the NSF MRL Program, DMR-79-23647

1. J. E. Fischer, Comm. Sol. St. Phys. 9, 93 (1979)

2. P. Bak, Physica 99B, 325 (1980)

3. S. Basu, C. Zeller, P. Flanders, C.D. Fuerst, W. D. Johnson and J.E. Fischer, Mat. Sci. Eng. 38, 275 (1979)

4. D. Guerard and A. Herold, Carbon 13, 337

5. N. Kambe, M.S. Dresselhaus, G. Dresselhaus, S. Basu and J.E. Fischer, Mat. Sci. Eng. 40, 1 (1979)

6. C. Ayache, E. Bonjour, R. Laguier and J.E. Fischer, Physica 99B, 547 (1980

7. S.A. Safran, Phys. Rev. Lett. (1980)

8. R. Nicklow, W. Wakabayashi and H.G. Smith, Phys Rev. B5, 4951 (1972)

9. W.D. Ellenson, D. Semmingson and J.E. Fischer, Mat. Sci. Eng. 31, 137 (1977)

10. J.E. Fischer, in Molecular Metals, W.E. Hatfield, editor Plenum, NY 1979) p 281

11. N.A.W. Holzwarth, L.A. Girifalco and S. Rabii, Phys. Rev. B18, 5025 (1978)

FIGURE CAPTIONS

Figure 1 — Elastic scans for LiC_6 at various temperatures and in various directions, as indicated. Indexing based on the Guerard cell (Ref. 4), with $\bar{a}$=4.30A, $\bar{c}$=3.71A. No stacking transition is observed down to 10K (see text).

Figure 2 — C-axis thermal expansion of LiC_6, as measured by the temperature variation of the (0,0,1) Bragg peak.

Figure 3 — Temperature dependence of the integrated (0,0,1) peak of stage 2, LiC_{12}. The sample eventually transforms entirely into a dilute stage 1 phase at 250°C. The remaining stage 2 intensity at 200°C is due to a dilute, slightly expanded stage 2 intermediate phase.

Figure 4 — Inelastic neutron energy loss spectra of LiC_6 at 200K, recorded for $\bar{q}$=0.1, 0.2 (the zone boundary is at $\bar{q}$=0.5). These are longitudinal modes propagating along $\bar{c}$.

Figure 5 — Dispersion of the two modes in Fig. 4. The upper branch is the LA mode, while the lower branch is tentatively assigned to an LO mode (see text).

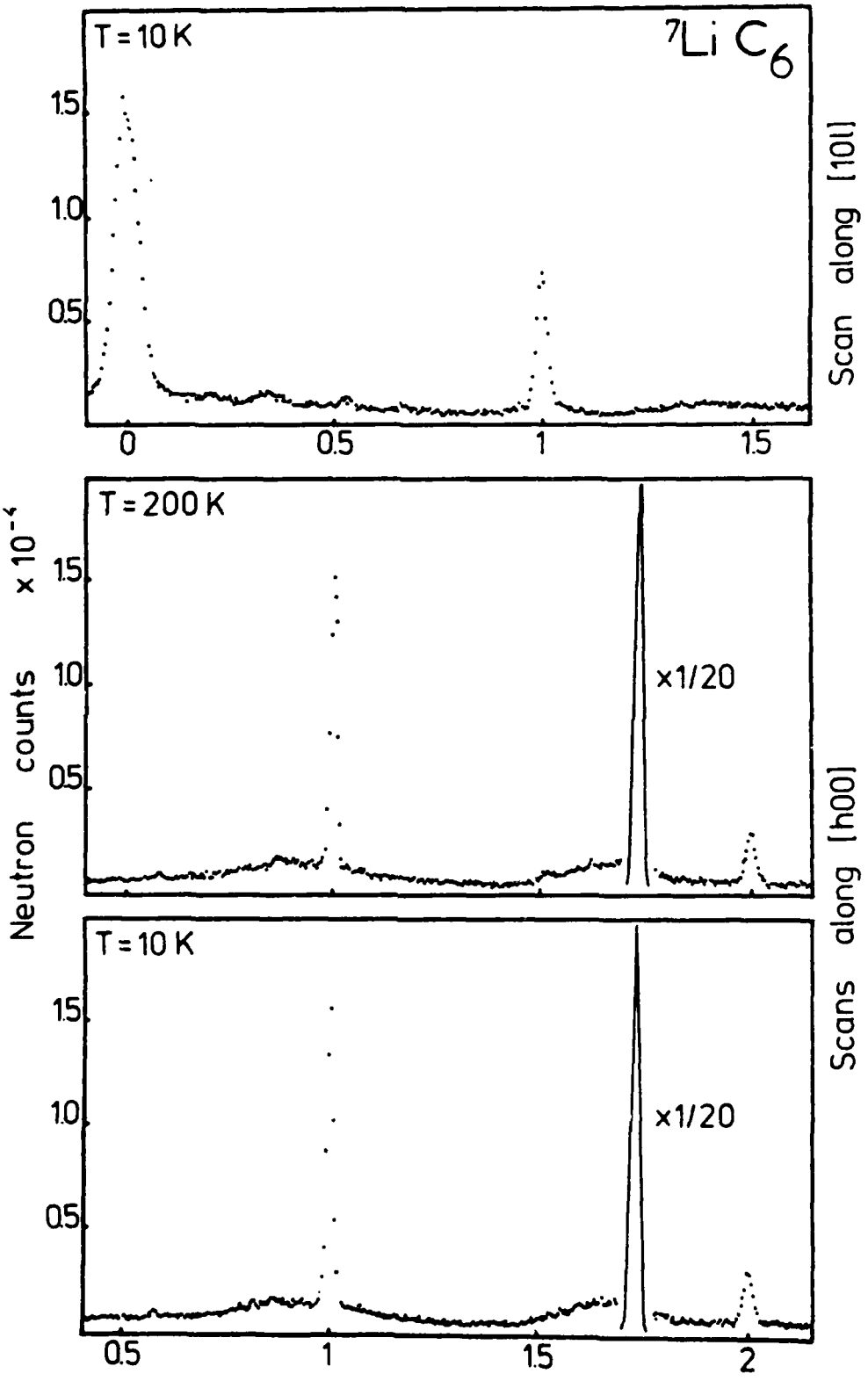

Rossat-Mignod et al. Fig 1

Rossat-Mignod et.al. Fig 2

Rossat-Mignod et.al. Fig. 3

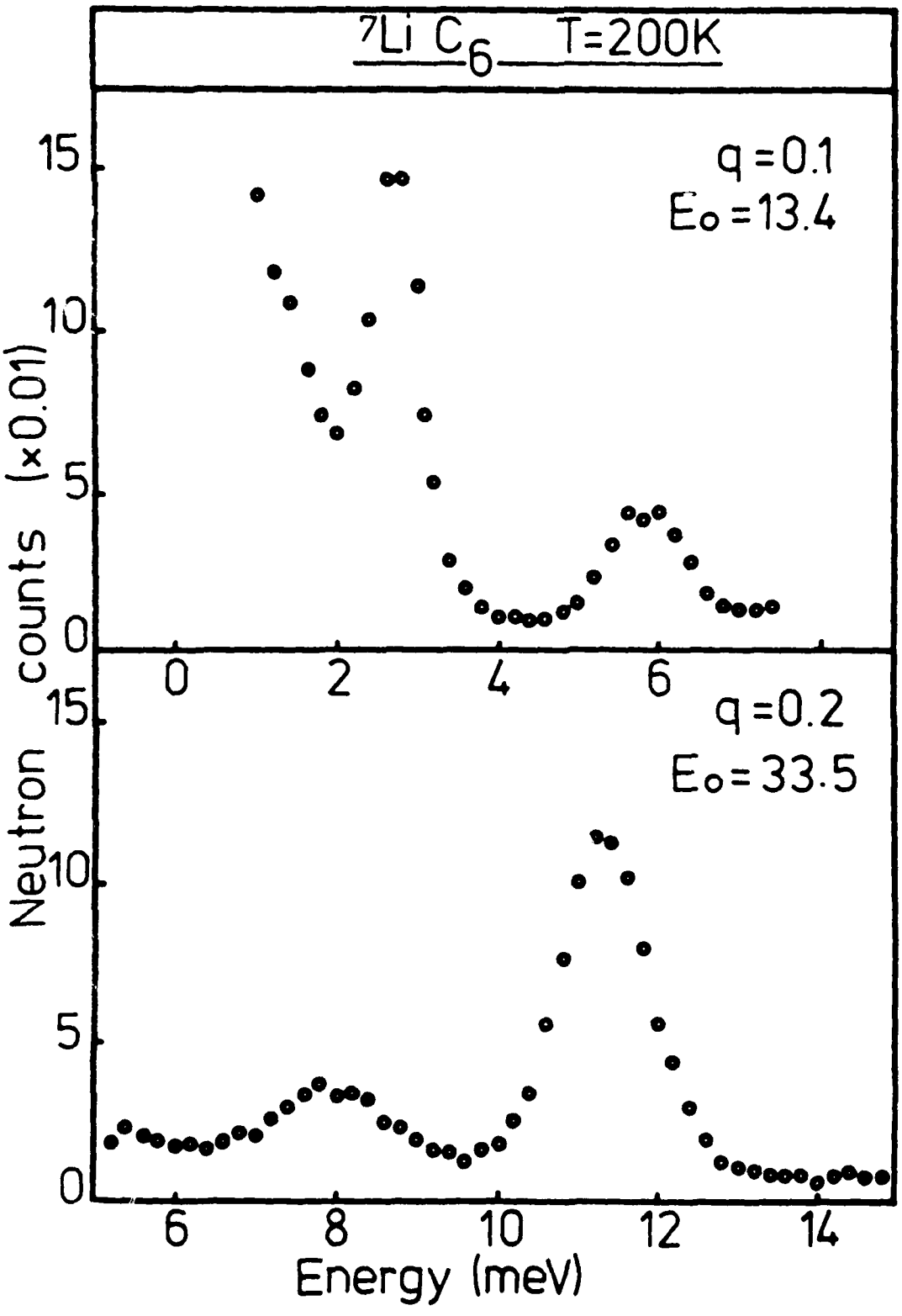

Rossat-Mignod et. al. Fig 4

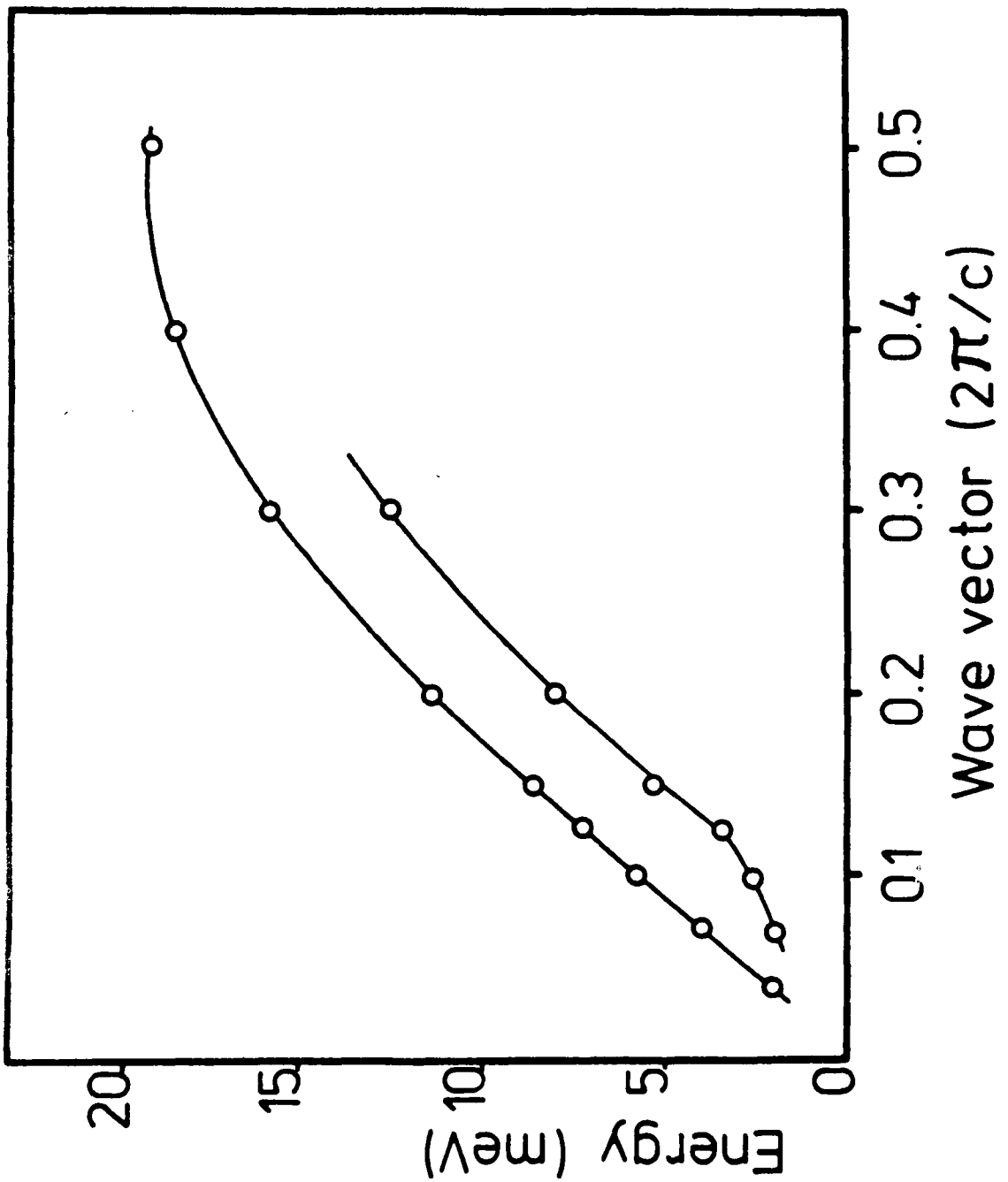

Rossat-Mignod et.al. Fig. 5

Elsevier Sequoia S.A., P.O. Box 851, 1001 Lausanne 1, Switzerland

SYNTHETIC METALS

MC

IN ALL CORRESPONDENCE CONCERNING THIS PAPER REFER TO

AUTHOR	X	EDITOR		MASTERCOPY		17 pages	SYM 107
QUERIES		CORRECTION		Vol. No. pp.			

Only typographical correction will be accepted at this stage.

Synthetic Metals,

A CALCULATION OF THE ELECTRONIC BAND STRUCTURE OF KC_8

D. P. DIVICENZO*, N. A. W. HOLZWARTH and S. RABII

Moore School of Electrical Engineering, University of Pennsylvania, Philadelphia, PA 19104 (U.S.A.)

(Received May 19, 1980)

Summary

Results of an *ab initio* band structure calculation for first stage potassium–graphite, KC_8, are presented along several high symmetry directions in the Brillouin zone. In the first step, we find the KKR band structure using the muffin tin approximation. In the second step we introduce the corrections to the muffin tin potential, leading to the final bands.

Our band structure, excluding the bands originating from the 3p and 4s levels of potassium, is in good agreement with the predictions of the folded band model of two dimensional graphite. The bottom of the K 4s band lies about 1.5 eV above the Fermi level. Preliminary indications are that our Fermi surface will lack the central, isotropic pocket of carriers predicted earlier, and will be more in agreement with the folded bands. We have also studied the lowest energy critical point transitions and find a series of saddle point transitions centered at 4.1 eV, roughly consistent with the experimental low energy electron loss spectra.

1. Introduction

First stage potassium–graphite, KC_8, continues to be a system under active experimental and theoretical investigation. In the last year alone, measurements of electron energy loss [1], angle integrated [2] and angle resolved [3] photoemission, de Haas–van Alphen periods [4], and electrical conductivity and Hall coefficient [5] have been performed. On the theory side, calculations of the electronic band structure and Fermi surface properties [6] and a KC_8 phonon spectrum [7] have been reported. The proximity of potassium states to the Fermi level of KC_8 makes an accurate band calculation difficult; we hope that our electronic structure work, based on a mathematically accurate *ab initio* technique, can provide a complete and accurate theoretical picture.

*IBM predoctoral fellow.

This paper serves as a brief progress report on our KC_8 band calculation. Section 2 presents KKR muffin tin bands throughout the Brillouin zone. Section 3 develops the method which we use to correct the muffin tin approximation, discusses some of the difficulties which we encountered, and gives the final bands obtained to date. Section 4 relates our results to some of the experiments mentioned above, considers this calculation in relation to previous ones, and speculates on work to be done in the near future.

2. Muffin tin energy bands

Our method of band structure calculation has been described previously [8, 9]. The plan of our work is as follows: A crystal potential is formed by the linear superposition of atomic charge densities for K^{+1} and $C^{-1/8}$. In the first step we use a muffin tin approximation to this potential; a constant outside the atomic spheres, the actual value inside. We calculate the scattering matrix $k^{\tau}{}_{lml'm'}$ and the KKR structure matrix $M^{\tau\tau'}{}_{lml'm'}$, then solve the secular equation:

$$\det \left[k^{-1}{}_{lml'm'}(E)\delta_{\tau\tau'} + M^{\tau\tau'}{}_{lml'm'}(\vec{k},E) \right] = 0 \qquad (1)$$

for wavevectors throughout the Brillouin zone. The result of this calculation is shown in Fig. 1.

Although the results of Fig. 1 are only approximate, they contain some physically useful information. First, we have discovered that for low energies (below about −0.3 Ry) the wave functions have relatively unmixed potassium or carbon character, so that the set of dispersionless bands at −1.39 Ry is clearly identifies as K 3p, the pair of bands with minimum at −0.48 Ry. (Γ_1^+) and −0.37 Ry (Γ_1^-) are derived from K 4s states, while the rest of the bands come from the states of pure graphite. Moreover, these graphite levels agree in many respects with those predicted by the folded band model. Figure 2 shows the energy bands of two dimensional graphite as calculated by Nagayoshi *et al.* [10] folded into the Brillouin zone of KC_8. A comparison of Figs. 1 and 2 shows that the graphite σ bands (shown solid) and most of the graphite π bands (dashed) survive with very little distortion in potassium–graphite. Also, all of the predicted band degeneracies shown in parentheses in Fig. 2 are correct for the KC_8 bands.

Still, there are certain aspects of the KKR muffin tin calculation which change significantly as a result of the muffin tin corrections. When compared with the actual crystal potential, the muffin tin potential is too attractive in the intercalant plane and too repulsive in the carbon plane. This means that the relative positions of the graphite π and σ bands, as well as that of the potassium and the graphite bands, are not given properly by this calculation. The potassium 4s level, for example, comes roughly two eV below the graphite Fermi level at −4.5 eV, in violent conflict with experiment. Thus it is pointless to attempt any further analysis — Fermi surface effects, optical properties, etc. — of our muffin tin bands.

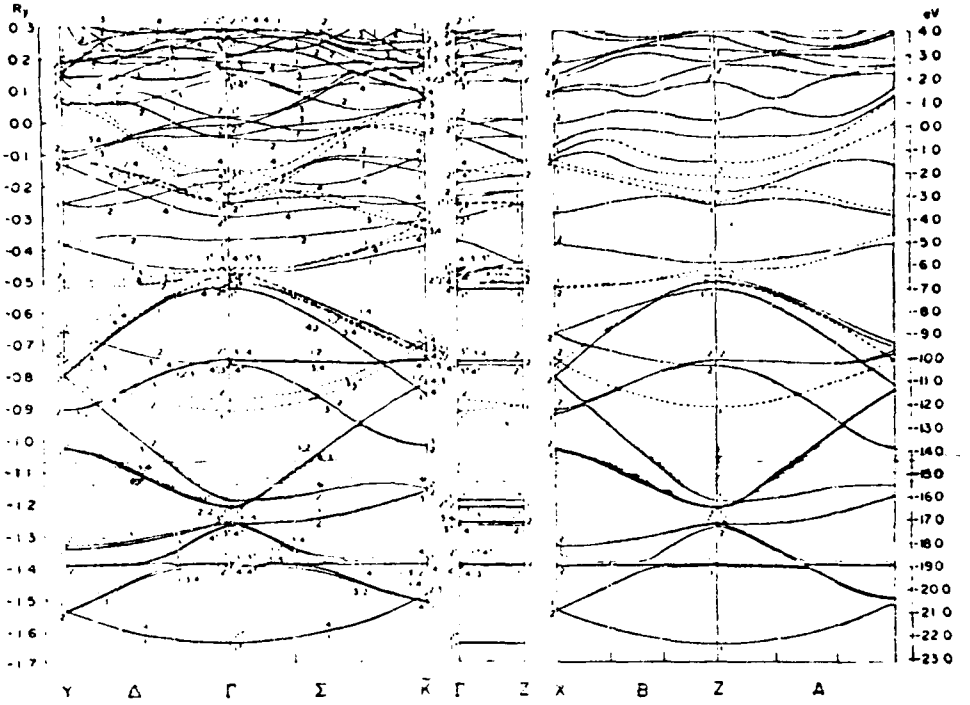

Fig. 1. The KKR muffin tin bands of potassium graphite. Bands derived from graphite π states are dashed; solid bands are graphite σ and potassium states.

3. Final KC_8 bands

The deviation of the full crystal potential from the muffin tin value in the interstitial region, $\Delta V(\vec{r})$, may be taken into account by calculating its matrix element between suitably normalized muffin tin wave functions $\psi_n(\vec{k},\vec{r})$:

$$\Delta_{nn'}(\vec{k}) = \int \psi_n^*(\vec{k},\vec{r})\, V(\vec{r})\, \psi_{n'}(\vec{k},\vec{r})\, d\vec{r} \qquad (2)$$

We now find the final energy eigenvalues of KC_8 by solving a second secular matrix:

$$\det\{\Delta_{nn'}(\vec{k}) + (E_n^{KKR}(\vec{k}) - E)\delta_{nn'}\}1 = 0 \qquad (3)$$

where E^{KKR} are all the energy eigenvalues calculated in the last Section within a range of 3Ry.

The evaluation of the matrix elements $\Delta_{nn'}(\vec{k})$ requires some discussion. For most high symmetry wavevectors the integral (2) need only be

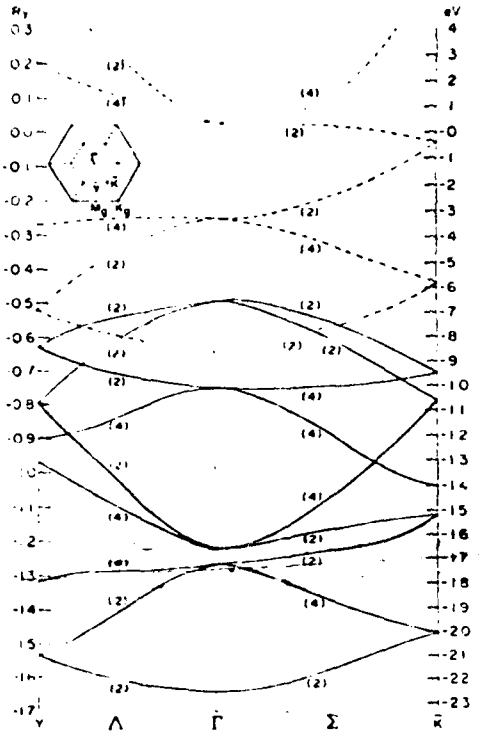

Fig. 2. Bands of two dimensional graphite folded into the Brillouin zone of KC_8. π Bands are dashed, σ bands solid. Numbers in parentheses indicate the band degeneracies. The insert shows the relationship between the graphite and KC_8 Brillouin zones.

evaluated in $\frac{1}{8}$ of the unit cell, the irreducible sector. Also, the integral is only non-zero in the interstitial region, which makes up only 43% of the crystal volume. However, the irregularity of this integration region (see Fig. 3) precludes the use of any of the standard numerical integration methods. We have developed a grid which approximates the integral (2) using Gaussian quadrature [11] in the three coordinate directions and which avoids the discontinuities caused by the irregular geometry. After considerable testing an integration grid containing 1675 points in the interstitial portion of the irreducible sector was used. Our previously published work [9] used a 483 point grid, which was not completely converged. Thus, the results reported were not absolutely correct. In our most recent work, numerical errors in $\Delta_{nn'}(\vec{k})$ are no greater than 0.03 Ry [12].

We have finished the solution of eqn. (3) for several wavevectors. Our results are shown in Fig. 4. Again, we show the graphite σ and potassium bands solid, the π bands dashed. The KC_8 band shapes still bear a close resemblance to the folded graphite bands of Nagayoshi *et al.* in Fig. 2. The relative positions of the graphite σ and π bands now agree very closely with

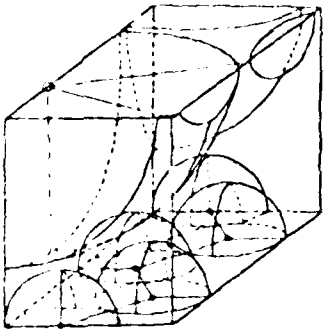

Fig. 3. KC_8 irreducible sector showing inscribed muffin tins of potassium and carbon.

the bands of two dimensional graphite folded into the KC_8 Brillouin zone. The potassium 3p levels appear as the flat set of bands at −1.39 Ry. The pair of bands with minima at −0.26 Ry (Γ_1^+) and −0.15 Ry (Γ_1^-) are derived from the K 4s levels. As expected, the potassium bands have shifted dramatically from their positions in the muffin tin calculation.

4. Discussion

Although we have completed our calculation for only a few $\vec{k}$ points in the Brillouin zone, we may draw several reasonable conclusions from them. The KC_8 Fermi level will fall at about −0.4 Ry on Fig. 4. The energy bands at this energy and below have very similar shapes to the folded graphite bands, although most of them are split by interactions with potassium states. We conclude that the density of states will be very similar to graphite's, and the Fermi surface will agree with that derived from the rigid band analysis performed by Holzwarth *et al.* [8]. This surface consists of rounded trigonal prisms centered at $\tilde{K}$ and equivalent wavevectors in the Brillouin zone. This differs from the Fermi surface calculated by Inoshita *et al.* [6] in that it lacks the roughly isotropic pocket of carriers centered at the Γ point; detailed calculations will be required to see if existing experimental results can be explained by our Fermi surface.

Table 1 gives the energies of the lowest energy critical point interband transitions at Γ, which are not critically sensitive to the exact position of the Fermi level. All the transitions shown derived from the M- point transition in the π bands of graphite reported at 4.5 eV [1], which is broadened and lowered in energy by the presence of the intercalant. Hwang *et al.* [1] have studied KC_8 using electron energy loss. They report a broad peak in $\epsilon_2(E)$ centered at 3.8 eV, in rough agreement with our results.

Future calculation should allow us to perform a more detailed analysis of Hwang's data, and to study other experimental results. As an example, Oelhafen *et al.* [2] have interpreted their photoemission data in terms of a partially filled potassium 4s band, in disagreement with our results. We hope to provide a new interpretation of their data.

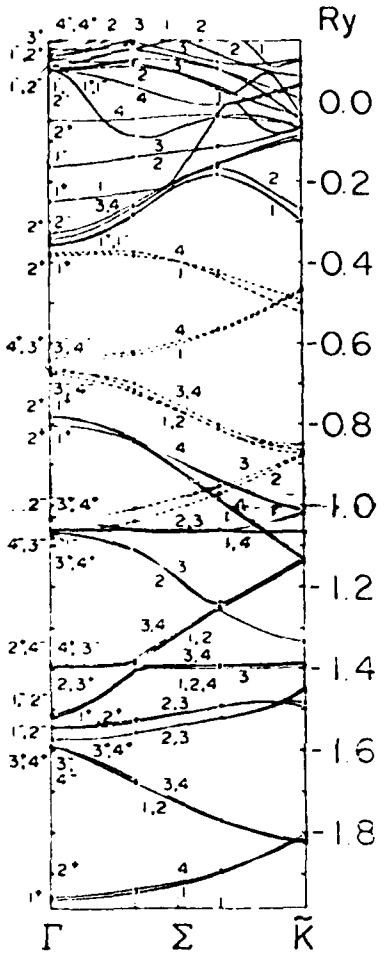

Fig. 4. Preliminary results of final corrected band structure of potassium graphite. π Bands are dashed, σ bands and potassium levels are solid.

Acknowledgments

The authors thank the members of the graphite group at Penn for ongoing close interactions. Thanks go to the Moore School Computing Facility for the use of their Univac 90/70 computer. This work was supported, in part, by the IBM predoctoral fellowship program, by ARO contract DAAG-29-77-C400 and by NSF on grant number DMR76-80994.

TABLE 1

Optical selection rules and principle low energy critical transitions for the Γ point in KC_8.

$1+ \overset{\parallel}{\leftrightarrow} 3-$	$3+ \overset{\parallel}{\leftrightarrow} 2-$	$2+ \overset{\perp}{\leftrightarrow} 1-$
$1+ \overset{\parallel}{\leftrightarrow} 4-$	$3+ \overset{\perp}{\leftrightarrow} 4-$	$4+ \overset{\parallel}{\leftrightarrow} 2-$
$1+ \overset{\perp}{\leftrightarrow} 2-$	$2+ \overset{\parallel}{\leftrightarrow} 4-$	$4+ \overset{\parallel}{\leftrightarrow} 1-$
$3+ \overset{\parallel}{\leftrightarrow} 1-$	$2+ \overset{\parallel}{\leftrightarrow} 3-$	$4+ \overset{\perp}{\leftrightarrow} 3-$

Transition at Γ	ΔE (eV)
$4- \rightarrow 2+$	3.4
$4- \rightarrow 1+$	3.5
$3- \rightarrow 2+$	3.5
$4+ \rightarrow 1-$	3.8
$3+ \rightarrow 1+$	3.9
$3+ \rightarrow 1-$	4.1
$4+ \rightarrow 1-$	4.2
$3+ \rightarrow 2-$	4.3
$4+ \rightarrow 2-$	4.5
$3- \rightarrow 2+$	4.7
$4- \rightarrow 2+$	4.8

References

1 D. M. Hwang, M. Utlaut, M. S. Isaacson and S. A. Solin, *Physica, B99* (1980) 435.
2 P. Oelhafen, P. Pluger, E. Huaser and H.-J. Günterodt, *Phys. Rev. Lett., 44* (1980) 197.
3 W. Eberhardt, personal communication.
4 H. Suematsu, S. Tanuma and K. Higuchi, *Physica, B99* (1980) 420.
5 W. D. Johnson, M. E. Potter and J. E. Fischer, *Bull. Am. Phys. Soc., 24* (1979) 410.
6 T. Inoshita, K. Nakao and H. Kamimura, *J. Phys. Soc. Jpn., 43* (1977) 1237; *45* (1978) 689; H. Kamimura, K. Nakao, T. Ohno and T. Inoshita, *Physica, B99* (1980) 401.
7 C. Horie, M. Meada and Y. Kuramoto, *Physica, B99* (1980) 430.
8 N. A. W. Holzwarth, S. Rabii and L. A. Girifalco, *Phys. Rev. B,18* (1978) 5190.
9 D. P. DiVincenzo, N. A. W. Holzwarth and S. Rabii, *Physica, B99* (1980) 423.
10 H. Nagayoshi, K. Nakao and Y. Uemura, *J. Phys. Soc. Jpn., 41* (1976) 2480.
11 F. B. Hildebrand, *Introduction to Numerical Analysis*, McGraw-Hill, New York, 2nd Edn., 1974, p. 379.
12 Our numerical technique is described in more detail in D. P. DiVincenzo, *Master's Thesis, University of Pennsylvania, 1980* (unpublished).

Elsevier Sequoia S.A., P.O. Box 851, 1001 Lausanne 1, Switzerland

SYNTHETIC METALS

AUTHOR	X	EDITOR		MASTERCOPY		8 pages	SYM 108.A
QUERIES	X	CORRECTION		Vol.	No.	pp.	

MC

IN ALL CORRESPONDENCE CONCERNING THIS PAPER REFER TO

Only typographical correction will be accepted at this stage.

Synthetic Metals,

ENERGY BAND STRUCTURE OF THREE DIMENSIONAL GRAPHITE

R. C. TATAR, N. A. W. HOLZWARTH and S. RABII

Moore School of Electrical Engineering, University of Pennsylvania, Philadelphia, PA 19104 (U.S.A.)

(Received May 19, 1980)

Summary

We present a progress report of our *ab initio* energy band structure calculation of 3-dimensional graphite. The motivation for this work derives from 2 principle objectives: (1) to provide a basis of comparison for our work on graphite intercalation compounds and, (2) further to test some computational aspects of our formalism. These considerations are discussed further in Section 1. In Section 2 we describe the graphite structure and our crystal potential. The formalism which has been presented in detail elsewhere [1] is briefly reviewed in Section 3. In Section 4 we present the results of our KKR calculation for a muffin tin potential. The final bands we have obtained so far are presented in Section 5 and we close with a comparison of our results with optical experiments and other theoretical studies.

1. Introduction

There have been many band structure calculations of graphite to date. The band structure of 2-dimensional graphite has been presented in refs. 2 - 6. The two dimensional model of graphite necessarily ignores interlayer interactions which introduce band splittings of roughly 1 eV and introduce important structure near the Fermi level.

The previous three dimensional calculations of the graphite band structure roughly fall in two categories. First there are the band structures which are fitted in detail to experimental results over a small energy range. These provide accurate information about the Fermi surface and are useful for correlating transport related measurements [5, 7] and explaining optical structure at moderate energies [8, 9]. The second category of three dimensional calculations cover a larger energy range and employ methods ranging LCAO [10, 11], pseudo-potentials [12] and original reformulations of combined OPW and tight-binding techniques [13]. In general, the accuracy of these calculations is not sufficient to expect an adequate representation of the Fermi surface of graphite. However, in ref. 13, a good representation obtained by tuning adjustable parameters of the model potential. Higher energy

optical properties are also better predicted. Reference 6 provides a good comparative review.

The work was initially undertaken to test the applicability of our procedure to graphite intercalation compounds. Because graphite represents a structurally limiting case, *i.e.*, highest geometric anisotropy of the crystalline graphite compounds, and given the vast body of literature on graphite, it was felt that it would provide the best test of our method.

2. Structure and potential

Graphite has the Bernal structure [14] (Fig. 1) with four atoms per unit cell: two each of the inequivalent A and B carbons. The space group of graphite is $P6_3/mmc$ — the subscript clearly displaying the non-symmorphicity. There are twenty four operations in the point group, which means that most of the calculations can be carried out be considering only 1/24th of the volume of the unit cell in an irreducible sector. The high anisotropy of the crystal structure naturally leads to a high anisotropy of the potential. This fact rules out any calculations based on a spherically symmetric or a purely muffin tin potential.

Our potential is computed in the following manner. First, a self-consistent atomic charge density for carbon is obtained using the Hartree–Fock–Slater formalism [15]. This incorporates the Slater Xα [16] approach to account for exchange/correlation effects. A linear superposition of atomic charge densities from each site is used to compute the crystal potential at any given point. The same Xα parameter [17], 0.759, is used in both the atomic and crystal potential calculations.

The resulting crystal potential is shown along three directions in Fig. 2. At a distance half the nearest neighbor spacing, the potential variation in the three directions shown is greater than 1 Rydberg. Clearly a muffin tin approximation will be very poor, so any use of such an approximation must be intermediate.

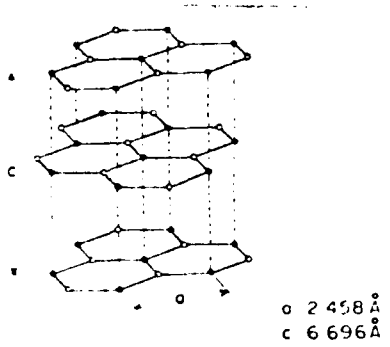

Fig. 1. Graphite crystal structure. ●, A carbons; ○, B carbons.

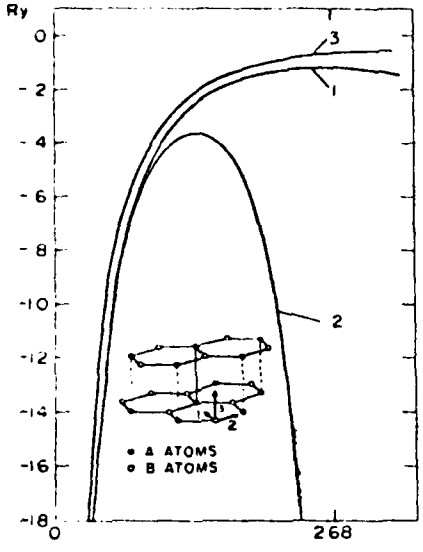

Fig. 2. Crystal potential of graphite.

The muffin tin potential that we use in the first step of our calculation is constructed from the actual potential in the following manner. Within touching spheres about each site (muffin tin radius) the actual potential is used. In the interstitial region, the potential is taken to be the volume averaged potential in that region (muffin tin zero). For graphite the muffin tin zero is −1.12 Ryd. The muffin tin radius is 1.84 a.u. and results in a 13% fractional fill of the unit cell by the muffin tin spheres.

3. Formalism

Our band structure calculation is a modified version of Painter's Discrete Variational KKR method [18]. In the conventional KKR formalism only the spherically symmetric component of the potential is retained. We generalize this method to include higher order terms in the angular momentum representation of the potential. This gives rise to a system of angular momentum coupled differential equations within the muffin tin spheres which we solve for a reaction matrix $K^{-1}_{lml'm'}$.

The reaction matrix is, in general, a complicated function of energy which we compute on a coarse energy grid. For graphite, we found that the reaction matrix components are very smooth functions of energy over the energy range considered, in contrast to previous calculations where singularities were present. [1, 19]. This smoothness makes possible rapid and very accurate numerical interpolation and extrapolation.

Our KKR equation takes the form:

$$[K^{-1\sigma}_{lml'm'}\cdot\delta_{\sigma\sigma'} + A^{\sigma\sigma'}_{lml'm'}]W^{l'm'}_{\sigma'} = 0$$

where K^{-1} is the reaction mateix, A is the structure matrix whose elements are evaluated with Ewald techniques and W are the coefficients in our KKR wave function. σ denotes the atomic site. The details have been presented in ref. 1.

To solve the KKR equation we write it as an eigenvalue equation:

$$[K^{-1\sigma}_{lml'm'}\cdot\delta_{\sigma\sigma'} + A^{\sigma\sigma'}_{lml'm'}]W^{l'm'}_{\sigma'} = \lambda(E)W^{lm}_{\sigma}$$

The eigenvalues $\lambda(E)$, are functions of the energy because the KKR matrix is energy dependent. The eigen energies which are physically meaningful correspond to the zeroes of $\lambda(E)$.

The accuracy of the KKR wave functions is limited by the spherical harmonic l truncation. Experience shows, however, that in many cases an s–p expansion is quite accurate and in almost all situations an expansion to d waves is extremely good. For graphite we have included components up to $l = 2$.

In graphite, all irreducible representations of groups of k vectors have explicit representations in terms of the atomic centered spherical harmonics to $l = 2$, making this truncation physically sufficient as well.

In a short test of the effect of the d-wave components, we recomputed the reaction matrix and KKR eigen energies excluding the $l = 2$ terms. We found that most of the bands shifted slightly but the doubly degenerate σ levels shifted more dramatically, reducing the separation between the occupied and unoccupied σ bands by more than 2 eV.

4. Muffin tin bands

By solving the KKR equation for many k-vectors along the edges of an irreducible sector of the 1st Brillouin zone (Fig. 3), we obtained bands shown in Fig. 4. Already many symmetry dependent features of the final bands are visible such as the touching π bands at K and the shape of the lower σ and π bands in the $k_z = 0$ plane which are characteristic of graphite.

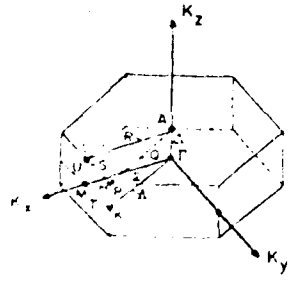

Fig. 3. Brillouin zone.

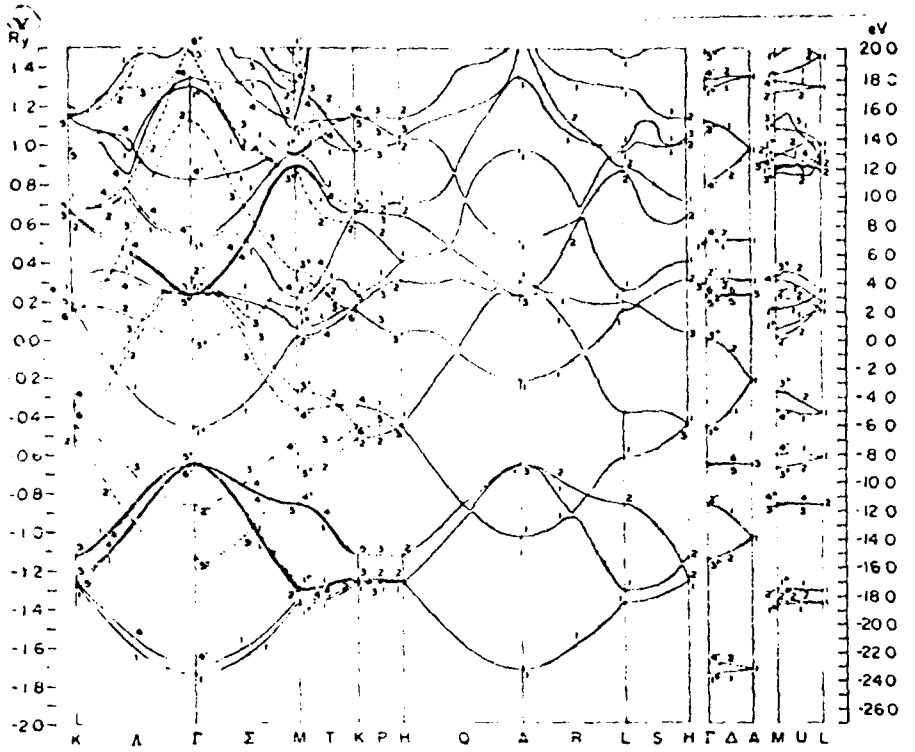

Fig. 4. Muffin tin bands of graphite (π bands are shown dashed).

The splitting of bands that are degenerate in single layer calculations is small but quite apparent. The muffin tin potential exaggerates this feature slightly and the splitting is reduced somewhat in the final bands. This can be explained as follows: Recalling the potential (Fig. 4) one sees that the muffin tin zero lies between the potential extrema of the directions parallel and perpendicular to the layers. Thus, in general, the c axis muffin tin potential is more attractive than that of the actual crystal and, conversely, the in-plane muffin tin potential is more repulsive on average. This means that the interlayer interactions (principally between p_z orbitals) — which are responsible for the splittings — are overestimated by the muffin tin potential. So one can expect the overall shapes of the bands perpendicular to the layer planes to be retained in the final results, but the dispersions along Δ, U and P to change more drastically. This appears to be borne out by our results so far. The occupied σ muffin tin band width at Γ is 16 eV compared with its final value of 14.7 eV — a change of less than 10% — showing the relative stiffness of the overall band shapes. At the K-pt however, the 3.2 eV splittling of the muffin tin π bands is reduced to about 1.6 eV in the final bands — the dispersion along P reduced by a factor of two.

5. Final non-muffin tin bands

To compute the final bands and eigenfunctions we first express the wavefunctions of a given symmetry as a linear combination of the muffin tin wavefunctions of the same symmetry. By diagonalizing the non-muffin tin hamiltonian — which is just the potential difference $V_{cr}^{(r)} - V_{mt}^{(r)}$, on this basis we arrive at a set of eigenvalues and eigenfunctions of the one electron problem for our crystal. This is we solve:

$$[E_n \delta_{nn'} + \Delta_{nn'}] C_{n'} = \epsilon C_n$$

where C_N are the coefficients of the new wavefunction,

$$\Delta_{nn'} = \int \psi_n (V_{cr} - V_{mt}) \psi_{n'} dr^3$$

$E_{nn'}$ is the eigen energy of the corresponding muffin tin wavefunction and E is the eigenvalue (energy) of the new wavefunction.

To compute the matrix elements $\Delta_{nn'}$ in this last step, the wavefunctions must be suitably normalized. Our normalization procedure is indirect but very efficient and is described in refs. 20 and 21. The final bands have been completed at Γ, M and at points along Λ, Σ and T. The most obvious effect of the non-muffin tin corrections is a general downward shift of approximately 0.3 Ryd for the entire energy bands. Some of the bands, however, behave very differently. In particular, the sigma ($\Gamma 1^+$) band moves up from the Fermi level into the higher conduction bands (Fig. 5).

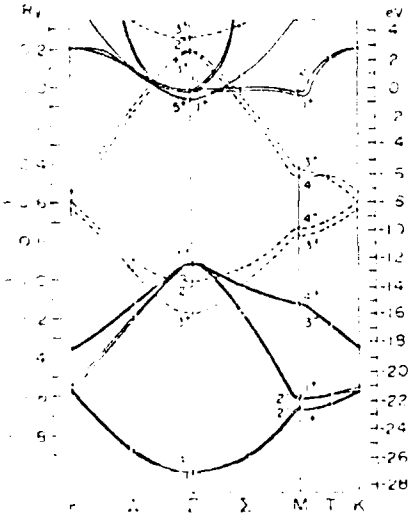

Fig. 5. Final band structure of graphite (π bands are shown dashed).

6. Discussion

Most of the previous band structure calculations obtain very similar values for certain features such as the 4.5 eV for M point π transitions, occupied σ bandwidth of nearly 16 eV, and $\pi-\sigma$ separation of around 12 eV. The present work is in general agreement with previous theoretical and experimental work as displayed in Table 1. In particular, the gap of 11.76 eV between the occupied and unoccupied σ bands at Γ and the separation of 11.3 eV between the lower σ and π bands are in excellent agreement with the experimental results. The corresponding values of the muffin tin bands are included to illustrate the dramatic difference between these and final bands.

Acknowledgments

The authors thank the University of Pennsylvania Graphite Group in general, and David P. DiVincenzo, in particular, for many stimulating discussions and helpful suggestions. Special thanks are due to the staff of the Moore School Computing Facility.

This work was supported, in part, by ARO contract DAAG-29-77-C400 and by NSF on grant number DMR76-80994.

TABLE 1

Comparison of graphite band structures

	KKR	Final	Willis [11]	Batra [10]	Zunger [9]	Exp.	Ref.
1. $\Gamma1^+ - \Gamma5^+$ σBW	16 eV	14.8 eV	15.8 eV	20.7 eV	16.5		
2. $\Gamma5^+ - \Gamma1^+$ occ.-unocc.	11.9	11.76	11.8	12.5	12.5	11.5 ± 1	11
3. $\Gamma3^+ - \Gamma3^+$ πBW	28	18.63	18	15	17.5		
4. $M3^+ - M4^-$ $M4^- - M3^+$	~4.4	~4.3	4.3	4.5	4.8	4.6	7
5. $\Gamma3^+ - \Gamma2^-$ πsep.	4	1.65	1.8	1.3	–	0.9 ± 0.3	22
6. $\Gamma1^+ - \Gamma3^+$	2.44	11.3	12	16	16	11 ± 0.3	22
7. K2 - K4	3.2	1.04	1.3	1.0	–	1.6	11

Bw = bandwidth.
sep. = separation.

References

1 N. A. W. Holzwarth, S. Rabii and L. A. Girifalco, *Phys. Rev. B,18* (1978) 5190.
2 W. M. Lomer, *Proc. R. Soc. London, Ser. A,277* (1955) 330.
3 F. Bassani and G. Pastori Parravicini, *Nuovo Cimento, 50B* (1967) 67.
4 G. S. Painter and D. E. Ellis, *Phys. Rev., B,1* (1970) 4747.
5 J. C. Sloncewski and P. R. Wiess, *Phys. Rev., 109* (1958) 272.
6 A. Zunger, *Phys. Rev. B,17* (1978) 626.
7 P. R. Wallace, *Phys. Rev., 71* (1947) 622; J. W. McClure, *Phys. Rev., 108* (1957) 612.
8 D. L. Greenaway, G. Harbeke, F. Bassani and E. Tosatti, *Phys. Rev., 178* (1969) 340.
9 L. G. Johnson and G. Dresselhaus, *Phys. Rev., B,7* (1973) 2275.
10 I. P. Batra, *Solid State Commun.* (submitted for publication)
11 R. F. Willis, B. Fitton and G. S. Painter, *Phys. Rev. B,9* (1974) 1926.
12 W. van Haeringen and H.-G. Junginger, *Solid State Commun., 7* (1969) 1723.
13 H. Nagayoshi, K. Nakao and Y. Uemura, *J. Phys. Soc. Jpn., 41* (1976) 1480.
14 J. D. Bernal, *Proc. Soc. London, Ser. A,106* (1924) 749.
15 F. Herman and S. Skillman, *Atomic Structure Calculations*, Prentice Hall, Englewood Cliffs, N.J., 1963.
16 J. C. Slater, *The Self Consistent Field for Molecules and Solids*, McGraw Hill, N.Y., 1974.
17 K. Schwartz, *Phys. Rev. B,5* (1972) 2466.
18 G. S. Painter, *Phys. Rev. B,7* (1973) 3520.
19 D. P. DiVincenzo, N. A. W. Holzwarth and S. Rabii, *Physica, 99B* (1980) 406.
20 N. A. W. Holzwarth, *Phys. Rev. B,11* (1975) 371B.
21 N. A. W. Holzwarth and M. G. Lee, *Phys. Rev. B,18* (1978) 5350.
22 I. T. McGovern, W. Eberhardt, E. W. Plummer and J. E. Fischer, *Physica, 99B* (1980) 415.
23 R. F. Willis, B. Feuerbacher and B. Fitton, *Phys. Rev. B,4* (1971) 2441.

TRANSPORT PROPERTIES OF ALKALI METAL-GRAPHITE INTERCALATION COMPOUNDS*

M.E. Potter+, W.D. Johnson** and J.E. Fischer

Moore School of Electrical Engineering
and
Laboratory for Research on the Structure of Matter
University of Pennsylvania
Philadelphia, Pennsylvania 19104

Basal resistivity ρ_a has been measured in situ on MC_8 compounds (M=K, Rb, Cs) from 5-300K. We find $\rho_a(T)=A+BT+CT^2$, in agreement with Suematsu et.al., except our value of A is ~200 times smaller implying fewer defects. In MC_8 compounds R_H at 5K is positive and increases linearly with magnetic field, suggesting a complex Fermi surface. On the other hand, R_H for RbC_{24} is negative and field-independent but the magnitude is inconsistent with a simple one-carrier model (assuming one free electron per Rb).

1. INTRODUCTION

The electronic transport properties of graphite intercalation compounds have been extensively studied,[1] with emphasis on the metallic conductivity exhibited by all compounds parallel to the layers (the a-direction). Alkali metal compounds are the simplest structurally, especially the stage 1 MC_8 materials (M=K, Rb, Cs) for which band structures have been calculated.[2] Despite their sensitivity to air, these compounds are amenable to standard galvanomagnetic techniques so that one can obtain reliable Hall effect and magnetoresistance data as well as resistivity.

Extensive studies on well-characterized samples based on HOPG (highly oriented pyrolytic graphite) were first performed by Murray and Ubbelohde[3] (MU). Their interpretation of R_H data for MC_8 compounds presumed a one-carrier Fermi surface which was subsequently shown to be incorrect,[4] and their analysis of $\rho_a(T)$ from 60-300K in terms of the usual Bloch-Gruneisen (BG) formula was not convincing. Suematsu et.al.[5] (SHT) measured $\rho_a(T)$ from 5-300K and found a good fit to $\rho_a(T) = A+BT+CT^2$, and proposed several explanations for the T^2 term. Their R_H data conflicted in sign, magnitude and temperature dependence with earlier work at Penn,[4,6] and their resistance ratios R(300K)/R(~5K) were considerably lower. In a series of papers the Penn group reported values of ρ_a, R_H and magnetoresistance at several fixed temperatures,[4,6] along with extensive measurements of transport anomalies in the stage 2 MC_{24} compounds.[6,7] Of these 3 sets of data, the MU and Penn results agree in the limited range where they overlap, but the SHT and Penn results are distinctly different. Thus it was deemed advisable to repeat some of the SHT experiments.

It is significant that both MU and the Penn group used *in situ* methods which avoid handling the samples after compound formation, while SHT transfer their samples from the preparation glassware into the measurement apparatus.

The only quality index available for comparing samples among the 3 groups is R(300)/R(77) for KC_8; the values are 11.4 (MU),[3] 5 (SHT)[5] and 11 (Penn).[4]

2. EXPERIMENTAL

All the samples studied were based on HOPG. Rectangular pieces 2.0 X 0.5 cm were cut using a diamond impregnated wire saw. These pieces were razor cleaved to a thickness of approximately 0.5mm and then cut into five-arm bridges by an air abrasive technique to minimize internal damage. The five-arm bridges were then tape cleaved to a thickness of approximately 0.2mm. The distance between voltage arms was 1.0cm with the Hall arm on the opposite side centered between the two voltage arms. Electrical connections were made with platinum wires and sintered gold contacts. The samples were then mounted in a specially designed pyrex rectangular envelope as described previously.[5] Vacuum-tight seals between the Pt wires and the pyrex were achieved with a soft intermediate glass. The open end of the rectangular pyrex was then joined to a long pyrex tube into which the alkali metal could be distilled. After distillation, the tube containing the alkali metal and the sample was sealed and the sample intercalated using the usual two-temperature method. Upon obtaining the desired stage, determined by color and (00ℓ) x-ray diffraction, the sample was sealed under vacuum.

Resistivity measurements were made using an ac current of 10mA at 33.3 Hz and lock-in detection in order to avoid thermal emf problems. The sample temperature was measured with a calibrated Si diode and controlled with an electronic temperature controller and heater. The temperature could be swept up or down at a controlled rate automatically. The voltage drop as a function of temperature was recorded by a semi-automated system. Hall data were obtained by sweeping H at fixed T.

3. RESULTS

The ρ_a values at 5K and 300K and their ratios are listed in Table I for KC_8, RbC_8, and CsC_8. For KC_8 and RbC_8 the present ratios are somewhat better than earlier Penn samples. For KC_8 SHT report one sample with $\rho_a(1.2) = 0.1$ μΩcm and three samples with $\rho_a(1.2)=0.1$ μΩcm. Thus their resistance ratios range from 3 to 60 times less than ours, assuming comparable values of $\rho_a(300)$.

The temperature dependence of ρ_a is shown in Fig. 1 for KC_8. Similar behavior was found for RbC_8 and CsC_8, these latter two being essentially identical and slightly more resistive than KC_8, as was found by MU. It is apparent that the data is not well-represented by the usual BG formula, which predicts $\rho \sim T^5$ at low T, $\rho \sim T$ at high T. Rather, the solid line in Fig. 1 is a linear least squares fit to $\rho_a(T) = A+BT+CT^2$ over the entire temperature range. The coefficients are listed in Table II.

In contrast to the stage 1 compounds, $\rho_a(T)$ for stage 2 compounds is quite linear[5-7] (except for the anomalies) over the range 80-300K. Here again, the Penn samples exhibit lower low-temperature resistivity than the SHT samples: for KC_{24}, $\rho_a(1.2) = 2.4$ μΩcm (SHT); $\rho_a(4.2) = 0.25$ μΩcm (Ref. 6). This may be significant in the comparison of Hall data to follow.

Figure 2 shows the field dependence of R_H ($\vec{H} \parallel \vec{c}$) at low temperature for KC_8, CsC_8 and RbC_{24}. It is clear that R_H is positive and varies approximately linearly with field for the stage 1 compounds, while $R_H<0$ and is field-independent for RbC_{24}. The latter is consistent with a single-carrier n-type metal, while the former suggests more complex behavior. The RbC_{24} R_H value is independent of T up to 300K, while R_H for the MC_8's is strongly temperature-dependent, as shown in Table III. The data newly reported here are consistent with earlier Penn group results[4,6] in showing that for MC_8 R_H changes sign from negative at

300K to positive in the helium range, in contrast to SHT. The sample-to-sample variations among the three Penn data sets are smaller than the variations observed by SHT.

Concerning the stage 2 compounds, Table III, both groups agree that R_H is negative at all temperatures, and that the temperature dependence of the magnitude of R_H is about a factor of 2 from 300K to ~4K (KC_{24},CsC_{24}). The Penn values are however consistently smaller by a factor of 3 or 4 than the SHT results. The magnitude discrepancy between SHT and Penn results gets worse as the samples get more dilute. For stage 3 KC_{36}, Onn et.al.[6] find R_H = -21×10^{-4} cm^3/ccul. while SHT report -280×10^{-4}; the respective values at stage 4 are -57×10^{-4} and either 80×10^{-4} or 1000×10^{-4} (sign not determined).

4. DISCUSSION

The $\rho_a(T)$ behavior of the MC_8 compounds is clearly unusual for such highly conducting materials. It is obvious from the $\rho_a(T)$ plots that no T^5 or linear-T regions occur in the three stage-one heavy-alkali-metal GIC's between 5K and 300K. It is unlikely that a T^5 region can be found below 5K since the residual resistivity seems to be dominant even at 5K. It would not be surprising however to find a linear-T dependence above 300K.

The reasons for the inconsistency between $\rho_a(T)$ and the BG theory are found in the assumptions which lead to the BG relation: the neglecting of
i) separate contributions from longitudinal and transverse phonon modes;
ii) electron-electron scattering and
iii) anisotropies in the Fermi surface.
The first of these is equivalent to neglecting U-processes which are dominated by transverse phonons. General carrier-carrier scattering cannot be overlooked, even though this contribution is only significant at very low temperatures for ideal metals.[8] Since the Fermi surfaces are partly two-dimensional[2] for KC_8 the

third assumption is definitely in error.

Table II indicates the temperature coefficients resulting from fitting to $\rho(T) = A + BT + CT^2$. The first term, A represents the residual resistivity and B is related to electron-phonon scattering. For the C term, two possibilities must be considered. First, since KC_8 has partially cylindrical Fermi surfaces, one is hopeful that Kukkonen's[9] extension of the BG theory for anisotropic metals could be applied. An estimate of when the T^2 dependence should begin can be done. For N-processes where longitudinal phonons are dominant, the onset temperature for T^2 behavior is $T(T^2)=230K$. Transverse acoustic phonons cannot be neglected without consideration, however. The transverse sound velocity of graphite (270m/s) yields $T(T^2)=15K$. It is therefore important to find out the relative weights of these processes in the compounds. Kukkonen did not have this problem with bismuth since in that case $T_{TA} \approx T_{LA}$. In this model the effective onset temperature must be far less than 230K for KC_8. The cutoff of the T^2 region is the Debye temperature, 234.8K for KC_8.[10] Θ_D is however an average value; the appropriate characteristic temperature may be above 300K. The experimental plots show no purely linear-T region below 300K.

In light of these facts, and since there are no $T^5 \rightarrow T^2 \rightarrow T$ transitions, a better explanation of the T^2 contribution might be the second possibility, general carrier-carrier scattering. Kukkonen et al. [11] also presented a theory of the effect of collisions between two types of charge carrier on the electrical resistivity of a simple degenerate semimetal. Although the theory was applied to TiS_2 (a layered compound with a hexagonal Brillouin zone and anisotropy of 10) it applies in general to any degenerate electron-hole system with spherical carrier pockets in which collisions between charge carriers conserve momentum. The result of this theory is a T^2 dependence for all temperatures. Whichever theory is more applicable, modifications will have to be made to

include the effects of the two different electron pockets of MC_8 compounds.

Several observations point to carrier-carrier scattering rather than anisotropy as the origin of the T^2 behavior in MC_8 compounds. First, the T^2 contribution is much stronger in stage 1 than in stage 2 compounds (the effective exponents of log-log plots are respectively 1.8 and $\sim$1 over the range 60-300K), whereas stage 2 is more highly anisotropic.[1] Second, the magnitude of the T^2 coefficient decreases in the sequence K:Rb:Cs, as does the density of electrons in the quasi-spherical pocket,[1,7] suggesting that the T^2 term might originate in collision between electrons from the spherical pocket and electrons (or holes) originating from the cylindrical Fermi surface pockets.

The B and C coefficients obtained for KC_8 are in general agreement with the SHT results, although they had some samples with much larger linear-T terms. The major discrepancy lies with the defect term A, as discussed previously.

A major effort was put forth in this work to obtain R_H values for stage 1 and 2 compounds, in light of the discrepancies between the recent SHT data[5] and earlier Penn results.[4] Once again we found $R_H > 0$ at low T for stage 1 compounds, in contrast to SHT. The discrepancy may be due to a predominance of defect-related phenomena in the SHT samples, which in turn may be related to the difference between in situ and ex situ techniques.

The sign change from <0 at high T to >0 at low T suggests that holes dominate at low T. The calculated Fermi surface does contain hole orbits throughout an appreciable portion of the zone, due to the connectivity of quasi-spherical and cylindrical electron pockets.[7] The hole orbits, centered at M and $\hat{M}$ points, show very small curvature over part of the trajectory, and thus may have very high mobility at low T. Another possible reason for the crossover from electron to hole dominance

could be a negative thermal expansion coefficient (as for graphite itself), in which case the basal plane contraction of the zone upon cooling would increase the fraction of c^* over which the two types of electron pockets are connected. This in turn would enhance the fraction of hole-type orbits. Note that the co-existence of electron and hole orbits evidenced by R_H would be consistent with electron-hole scattering as the origin of the T^2 term in ρ_a.

A second point of contention between the Penn and SHT results is whether or not R_H for stage 2 compounds is consistent with a single-carrier model.[1,4] The metal atom densities are $\sim 3.5 \times 10^{21}/cm^3$ in MC_{24} (M=K, Rb, Cs), so the minimum absolute value of R_H (equivalent to one free electron per M atom) is $\sim 20 \times 10^{-4}$ $cm^3/coul$. Referring to Table III, this limit appears to be satisfied by KC_{24} and CsC_{24} at 4K, but not by RbC_{24}, at any T nor by the others at T>77K. A slight departure from ideal one-carrier behavior might be simply due to the "trigonal warping" of the cylindrical electron surfaces.[2] Of the three compounds, only RbC_{24} exhibits an R_H which decreases in magnitude with decreasing T, resulting in a major departure from the one-carrier limit at 4K.

The differences between electron/atom ratios (or fractional ionization) inferred from the Penn and SHT data are substantial. For KC_{24} f=1.1 (Penn) or 0.3 (SHT); for KC_{36} f=1.1 (Penn) or 0.1 (SHT); for KC_{48} f=0.6 (Penn) or 0.03-0.3 (SHT). We also find $f \sim 1$ for CsC_{24}[6] and CsC_{36}.[4] Many other experiments are consistent with f=1 for stage 2 and higher alkali metal compounds.[1] We suggest again that the difference may arise from differences in sample handling technique.

Since the galvanomagnetic properties are so complex, their detailed interpretation will have to incorporate the subtle features of the Fermi surfaces. Establishing the latter requires testing the band structure-derived Fermi surface

with quantum oscillatory experiments such as the de Haas-van Alphen effect. SHT have performed such experiments on the same specimens used in their galvanomagnetic studies.[13] The values of f inferred from the dHvA results are $\sim$0.2 for KC_{36} and KC_{48}. Similar *in situ* experiments on our samples are in progress.

REFERENCES

* Supported by ARO Contract DAAG29-77C-0040 and by the NSF MRL Program through Grant DMR-7923647.

+ Current Address: Bell Labs, Allentown, PA.

** Current Address: Dow Chemical Co., Midland, MI.

1. FISCHER, J.E. in "Intercalated Layered Materials", LEVY, F., editor (REIDEL, D. Dordrecht 1979) p 481; SPAIN, I.L., in "Physics and Chemistry of Carbon", Walker and Thrower, editors (in press); DRESSELHAUS, M.S. and DRESSELHAUS, G., Advances in Physics (in press).
2. INOSHITA, T., NAKAO, K., KAMIMURA, H. , J. Phys. Soc. Japan 43, 1237(1977).
3. MURRAY, J.J., and UBBELOHDE, A.R., Pro. Roy. Soc. A 312, 371 (1969).
4. GUERARD, D., FOLEY, G.M.T., ZANINI, M., FISCHER, J.E., IL NUOVO CIMENTO 38, 410 (1977).
5. SUEMATSU, H., HIGUCHI, K., TANUMA, S., J. Phys. Soc. Japan, 48, 1541 (1980).
6. ONN, D.G., FOLEY, G.M.T., and FISCHER, J.E., Phys. Rev. B19 6474 (1979).
7. ONN, D., FOLEY, G.M.T., FISCHER, J.E., Mat. Sci. & Eng. 31, 271 (1977).
8. ZIMAN, J.M., Electrons and Phonons, (Oxford University Press, London, 1960) p 415.
9. KUKKONEN, C.A., Phys. Rev. B 18, 1849 (1978).
10. KONDOW, T., MIZUTANI, U., MASSALSKI, T.B., Mat. Sci. & Eng. 31, 267 (1977).
11. KUKKONEN, C.A. and MALDAGUE, P.F., Phys. Rev. Lett. 37, 782 (1976).
12. BORSIER, C., Thèse d'Etat, Orleans 1978 (unpublished).
13. HIGUCHI, K., SUEMATSU, H., and TANUMA, S., J. Phys. Soc. Japan 48, 1532,(1980).
14. SUEMATSU, H., TANUMA, S., and HIGUCHI, K., Physica 99B, 420 (1980).

TABLE I

	ρ_a(300K) ($\mu\Omega$ cm)	ρ_a (5K) ($\mu\Omega$ cm)	$\frac{\rho_a(300K)}{\rho_a(5K)}$
KC_8	9.30	0.33	282
RbC_8	9.02	0.04	226
CsC_8	8.54	0.05	184
KC_8 (REF. 6)			218
KC_8 (REF. 5)			5-180
RbC_8 (REF. 4)			120

TABLE II

	A 10^{-9} Ω cm	B 10^{-9} Ω cm/K	C 10^{-11} Ωcm/K^2
KC_8	8.355	3.402	9.336
RbC_8	9.659	7.098	7.633
CsC_8	40.56	7.264	6.974
KC_8 (REF. 14)	1860	7.5	15.3

TABLE III

R_H@ 20kG (10^{-4} cm^3/coul.)

		THIS WORK	REF 6	REF 4	REF 5 (SHT)
KC_8	~4K 77K 300K	+3.2 (-0.3)	+4.5 -1.1 (-1.4)	 -0.8 	-12, -3.2 -1.2, -3.7 >0
RbC_8	~4K			+4.8	
CsC_8	~4K 77K 300K	+7.3 (-0.3)		 -0.48 (-1.8)	
KC_{24}	~4K 77K 300K		-16 -12.3 - 8.8		-63. -49. -28.
RbC_{24}	~4K 77K 300K	-7.2 -8.0 -8.0		 -7.7 -8.0	
CsC_{24}	~4K 77K 300K		-19. -19. - 8.0		
KC_{36}	~4K		-21		-280
KC_{48}	~4K		-57		80, 1000

Table Captions

Table I — Basal resistivity ρ_a at 300K and 5 K for stage 1 alkali metal compounds. The ratio is a rough index of sample quality. Ratios from previous publications are included.

Table II — Parameters obtained from fitting $\rho_a = A + BT + CT^2$. Data from Ref. 14 is included for KC_8.

Table III — Hall coefficients measured at $\sim$20 kG at several temperatures for a variety of alkali metal compounds. Earlier data are included for comparison. Values in parentheses are upper limits only. The sign of R_H for KC_{48} was not determined in Ref. 5.

Figure Captions

Figure 1 — Basal resistivity ρ_a versus T for KC_8 (in situ 4-wire measurement). The solid line is a linear least squares fit to $\rho_a = A + BT + CT^2$ (fit parameters listed in Table II). The semilog scale exaggerates the discrepancy between data points and the linear fit below 50K.

Figure 2 — Hall coefficient versus magnetic field ($\bar{J} \parallel \bar{a}$, $H \parallel \bar{c}$) for KC_8, CsC_8, and RbC_{24} at low temperature. With a constant voltage error, the R_H error decreases with increasing $\bar{H}$.

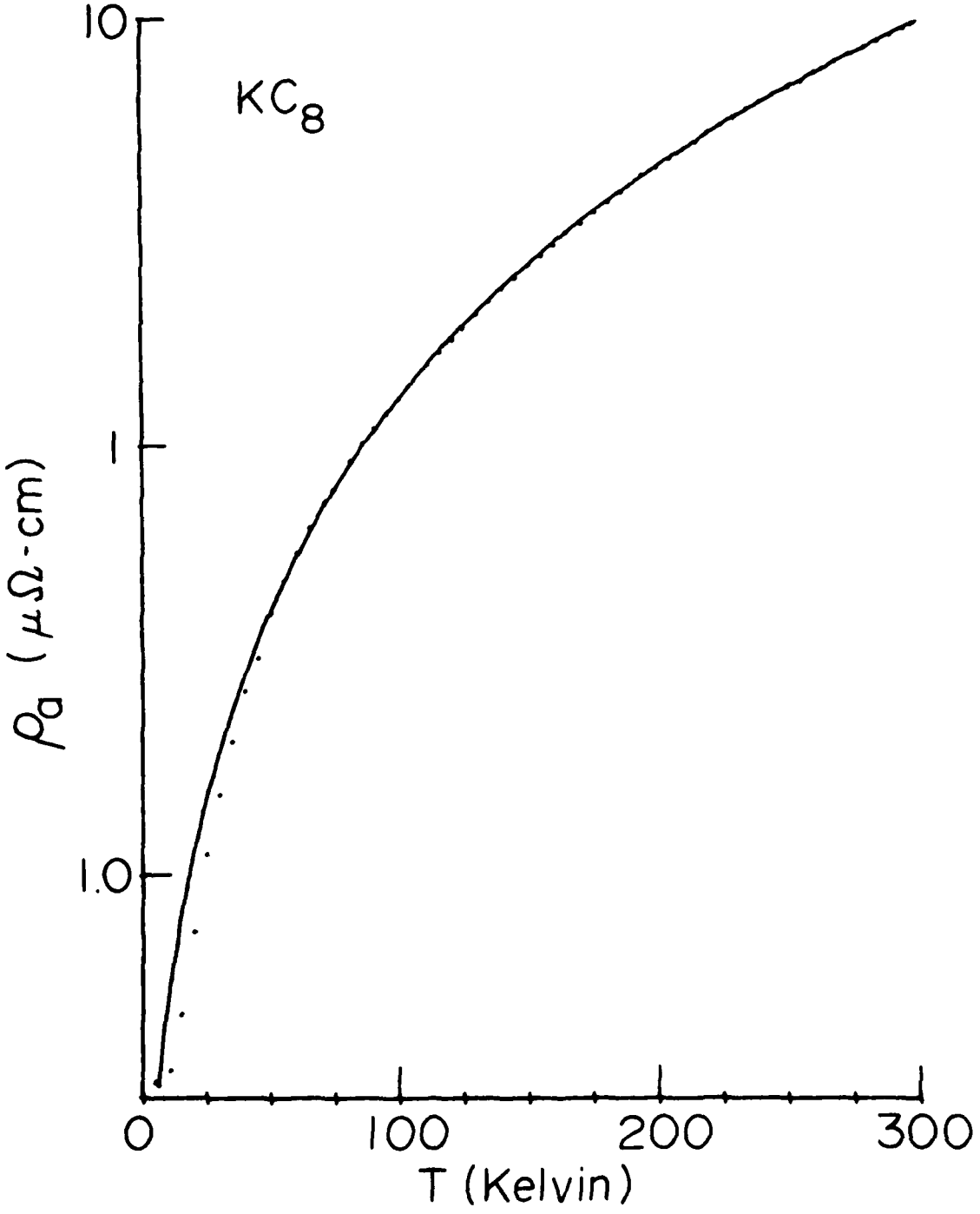

Potter et.al. Fig. 1

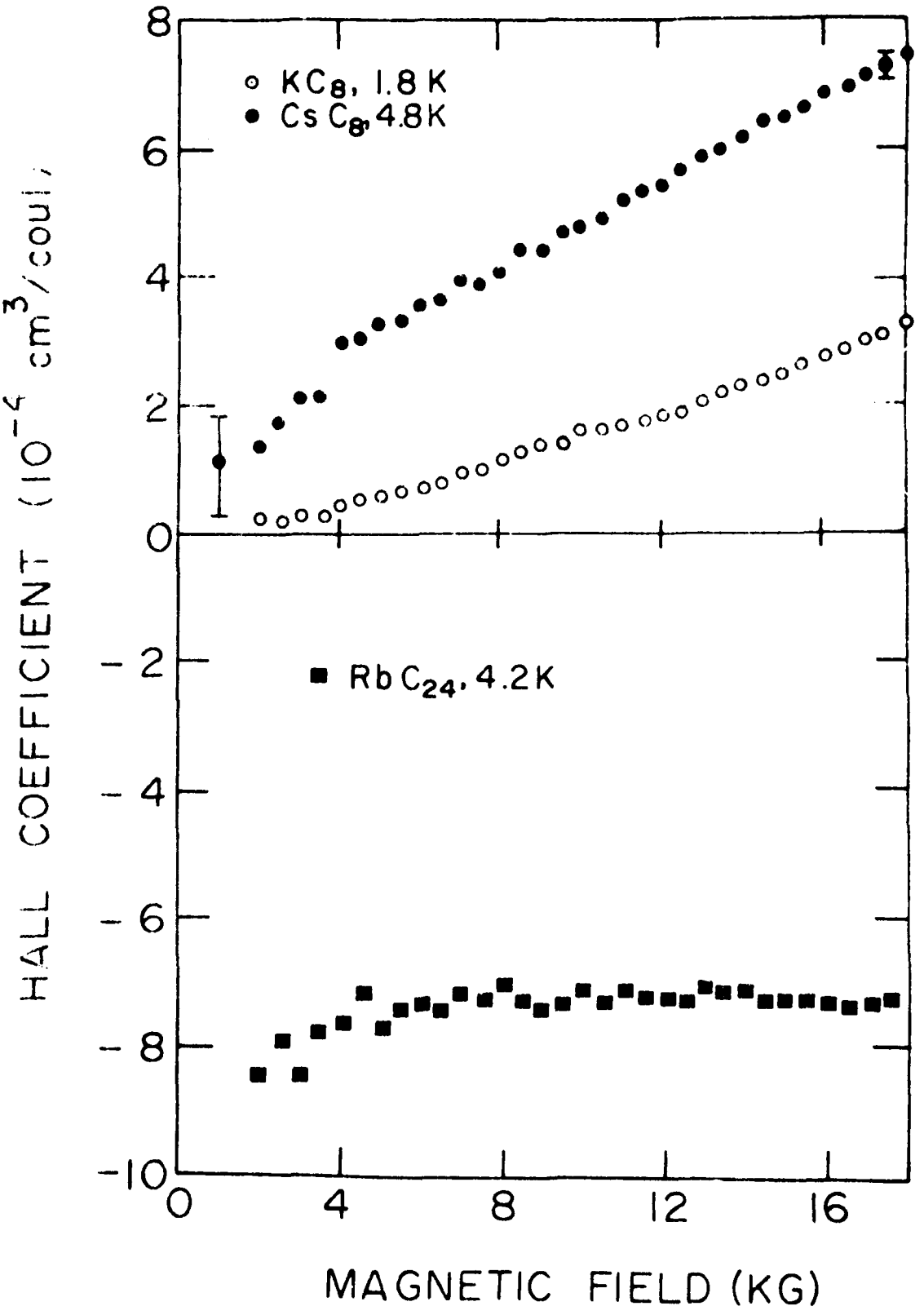

Potter et.al. Fig. 2

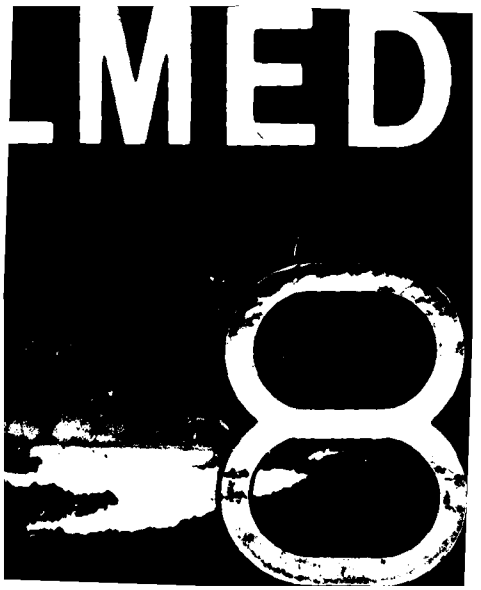
LMED
8